Effect of High-Fidelity Ice Accretion Simulations on the Performance of a Full-Scale Airfoil Model

Andy P. Broeren[*] and Michael B. Bragg[†]
University of Illinois, Urbana, Illinois, 61801

Harold E. Addy, Jr.[‡]
NASA Glenn Research Center, Cleveland, Ohio, 44135

Sam Lee[§]
ASRC Aerospace Corporation, Cleveland, Ohio, 44135

Frédéric Moens[¶]
ONERA, Meudon, France F92190

and Didier Guffond[#]
ONERA, Châtillon, France F92322

The simulation of ice accretion on a wing or other surface is often required for aerodynamic evaluation. While there are commonly accepted practices for conducting this work, there are no established and validated guidelines. The purpose of this paper was to report the results of a study to establish a set of high-fidelity, full-scale, iced-airfoil aerodynamic performance data. These data were acquired as a part of a larger program with the goal of developing subscale simulation methods for ice accretion. Airfoil performance testing was carried out at the ONERA F1 pressurized wind tunnel using a 72-inch (1828.8-mm) chord NACA 23012 airfoil over a Reynolds number range of 4.5×10^6 to 16.0×10^6 and a Mach number range of 0.10 to 0.28. Selected for testing were six, high-fidelity, ice-casting simulations classified by their aerodynamic effect. There was one horn shape, one spanwise-ridge shape, two streamwise shapes and two roughness shapes. The ice-shape simulations had a significant effect on the aerodynamic performance. The spanwise-ridge shape resulted in a maximum lift coefficient of 0.56 compared to the clean value of 1.85 at $Re = 15.9 \times 10^6$ and $M = 0.20$. The two roughness and streamwise shapes yielded maximum lift values in the range of 1.09 to 1.28, which was a relatively small variation compared to the differences in the ice geometry. The stalling characteristics of the two roughness and one streamwise ice simulation maintained the abrupt leading-edge stall type of the clean NACA 23012 airfoil, despite the significant decrease in maximum lift. Changes in Reynolds and Mach number over the large range tested had little or no effect on the iced-airfoil performance. This result indicates that subscale aerodynamic simulation may be quite successful.

I. Introduction

In many applications the simulation of the ice accretion geometry on a wing or other surface is required for aerodynamic evaluation. The measurement of aerodynamic performance from an aircraft or wing with actual ice accretions is very difficult and expensive and seldom a practical solution. Aircraft performance with ice accreted in flight are available,[1-3] but limited, due to the cost and difficulty in acquiring these data. In flight it is difficult to

---

[*] Research Scientist, Department of Aerospace Engineering, Associate Fellow AIAA.
[†] Professor of Aerospace Engineering and Associate Dean for Research and Administrative Affairs, Fellow AIAA.
[‡] Research Engineer, Icing Branch, Associate Fellow AIAA.
[§] Research Engineer, Icing Branch, Member AIAA.
[¶] Research Engineer, Applied Aerodynamics Department, Member AIAA.
[#] Specialist Research Engineer, Instrumentation and Sensing Department, Atmospheric Environment Research Unit.

document the ice accretion geometry accurately, where shedding often occurs, the accretions are for variable cloud conditions, etc. For accretions formed in an icing wind tunnel the inability to provide adequate instrumentation, nonuniformity of the cloud over the model, poor aerodynamic flow quality, and cost also make aerodynamic measurements difficult and rare. The most common way to acquire iced-airfoil and wing data is to use simulated accretions in a dry-air wind tunnel, or in flight. This process requires methods for developing the ice accretion simulations. While there are commonly accepted practices supported by research in this area, there are also remaining questions about the accuracy of such simulations.

Many of these open issues are directly addressed in the "Airfoil Ice-Accretion Aerodynamics Simulation" research program sponsored by NASA and ONERA.[4] The completed program will result in validated scale model simulation methods that produce the essential aerodynamic features of the full-scale iced airfoil. A review of the existing iced-airfoil aerodynamic literature was performed in order to classify ice shapes according to their aerodynamic effects. Four categories of ice accretion were defined: roughness, horn, streamwise and spanwise ridge. Ice accretion and follow-on aerodynamic testing were performed on subscale (18-inch (457.2-mm) chord, NACA 23012 airfoil) models for one ice accretion in each of the four categories. The purpose of the aerodynamic testing was to quantify the accuracy associated with various ice accretion simulation methods, from the highest fidelity ice castings down to simple geometric representations. The small model scale allowed for inexpensive investigations of a variety of simulation methods. Ice accretion and follow-on aerodynamic testing were also conducted on full-scale (72-inches (1828.8-mm) chord, NACA 23012 airfoil) models. The ice-casting simulations were applied to the model leading edge and the aerodynamic performance was acquired over a large range of Reynolds and Mach number. These data provided the necessary validation data for the methods developed in the subscale testing. This paper presents the results of the full-scale aerodynamic testing. Preliminary results of this program have been presented in previous papers.[5-11]

The full-scale aerodynamic testing was carried out using cast ice accretion simulations. The mold and casting method developed at NASA Glenn[12] is considered the best current technology for accurate ice accretion simulation. In this method molds are made from ice accretion generated in the NASA Icing Research Tunnel (IRT), or other icing tunnel. From these molds ice accretion castings are made that maintain the major features of the ice including the detailed surface roughness and the spanwise and chordwise variations. These castings have been attached to wings and airfoils, and instrumented to obtain high-fidelity aerodynamic data.[13-15] This is an expensive process and not practical for many situations, but was required to generate the benchmark data for this research program.

The ice accretion testing was designed to yield accretions that were closely aligned with the classifications developed by Bragg et al.[5,6] The four categories were based upon the aerodynamic and flowfield characteristics of the ice accretions. For example, roughness is defined as the type of ice accretion that affects the boundary-layer transition process, extracting momentum from the boundary layer leading to premature trailing-edge separation and increasing drag and reducing lift. There is local boundary-layer separation on the scale of the individual roughness elements. Horn ice is a larger accretion that has at least one protrusion orientated at a large angle to the oncoming flow and is located in the airfoil leading-edge region such that the stagnation point is on the ice accretion. This results in a large separation bubble aft of the accretion that governs the aerodynamics. The separation bubble significantly increases the drag and reduces the stalling angle of attack and maximum lift. Streamwise ice is more conformal to the leading edge and thus does not result in a large separated flow region. There may be localized separation on the scale of the ice shape owing to discontinuities at the ice/airfoil junction. The boundary layer is significantly affected by the ice, resulting in earlier transition and trailing-edge separation. Spanwise-ridge ice is characterized by a large separation bubble aft of the ridge, but differs from horn ice in that ridges are located downstream of the leading edge. The airfoil upstream of the ice ridge is smooth such that the stagnation point is not located on the ice accretion, and a boundary layer develops upstream. This leads to an additional separation bubble upstream of the ridge thus making the three-dimensional characteristics of the ridge more important than in the horn ice case. It is important to note that there is often overlap among these classifications and that real ice accretion could be characterized by a combination of these descriptions. However, this type of flowfield-based understanding is useful from the simulation perspective. Thus, it was this understanding that guided the selection of full-scale ice accretions for the aerodynamic testing presented in this paper.

While much of our understanding of ice accretion aerodynamics is anchored by cast ice simulation data, there have been very few studies employing full-scale ice accretion cast shapes aerodynamically tested at full-scale Reynolds number and Mach number. The second FAA/NASA Tailplane Icing Program provides full-scale, cast-ice performance data at full-scale Reynolds and Mach number, but the ice shapes were applied to a fully three-dimensional tailplane model.[16] The NASA Modern Airfoils Program[17] currently provides the best airfoil performance data set at flight Reynolds and Mach numbers, but due to size limitations in the NASA Low-Turbulence Pressure Tunnel (LTPT) used for the aerodynamic testing, the ice accretions were obtained on a 36-inch

(914.4-mm) chord airfoil. Ice accretion scaling methods can provide scaling of the gross ice shape for moderate scales,[18] but not of the roughness and ice shape details known to be aerodynamically important in some cases.

Therefore, the purpose of the full-scale aerodynamic testing was to establish a set of high-fidelity benchmark data useful for the development of simulation methods for smaller scale.   Airfoil performance testing was carried out at the ONERA F1 pressurized wind-tunnel using a 72-inch (1828.8-mm) chord NACA 23012 airfoil over a Reynolds number range of 4.5×10^6 to 16.0×10^6 and a Mach number range of 0.10 to 0.28. A total of six different ice accretion casting simulations were tested. The aerodynamic effect of the simulated ice accretion on the airfoil was documented through measurement of the performance and flow visualization. The purpose of this paper is to present these results.

II. Experimental Methods

All of the aerodynamic testing was performed at the ONERA F1 full-scale, pressurized wind-tunnel facility.[19] The closed-return wind tunnel has a test-section measuring 138-inches (3500-mm) high by 177-inches (4500 mm) wide by 433-inches (11000-mm) long. The maximum test section Mach number is 0.36 and the maximum stagnation pressure is 57 psia (3.85 bar). The unit Reynolds number can be varied up to a maximum of 6.0×10^6/ft at Mach = 0.23. Total temperature is maintained via a heat exchanger located in the second diffuser downstream of the fan. The fan operates at constant speed while the test section Mach number is controlled by adjusting the pitch of the blades.   The test-section inlet flow is conditioned through a 7.18-to-1 contraction containing honeycomb flow straightener and three turbulence reduction screens.

The 72-inch (1828.8-mm) chord NACA 23012 airfoil model was mounted vertically in the test section as shown in Fig. 1. The model span was 137.48-inches (3492-mm) and was mounted in the floor force balance. Small gaps between the bottom of the model and the test-section floor as well as the top of the model and the test-section ceiling were maintained so as not to cause mechanical hysteresis in the force-balance measurements. The model had a main chordwise row of 72 pressure taps located at 43% span measured from the test-section floor. In addition, there was a row of 20 taps oriented spanwise at $x/c = 0.70$ on the upper surface. The model was designed and built with full-span removable, interchangeable leading-edge sections. The baseline leading edge had the clean NACA 23012 profile, while the alternate leading edge had a truncated nose geometry. The latter design facilitated mounting of the various ice-shape casting simulations. Accommodations were also made in the pressure tapping to allow for rapid connection of pressure instrumentation in the cast ice shapes. Also shown in Fig. 1 is the wake rake located one chord length downstream of the model trailing edge. The wake rake had 100 stagnation pressure probes spaced 0.79-inch (20-mm) apart and was located at a fixed spanwise station at 57% span above the test-section floor.

Fig. 1 Photograph of NACA 23012 airfoil model installed in ONERA F1 wind-tunnel test section.

Data acquisition runs were performed in angle of attack sweeps for increasing and then decreasing angle of attack at a constant sweep rate of 0.1 deg./sec. Data were also acquired at fixed angle of attack for selected angles over the range of the sweep and repeat runs were performed to ensure data precision. The data shown in this paper are for increasing angle of attack sweeps and have been averaged to the nearest 0.5 deg. in post-processing. During the sweeps, data were acquired from the force balance and tunnel conditions analog transducers. The model surface, test-section sidewall, and wake-rake pressures were acquired using an electronically scanned pressure system. The acquisition of these data were synchronized in time corresponding to the angle of attack sweep rate. Lift and pitching-moment coefficients were calculated from the force balance and from the integration of the surface pressure measurements. Good agreement between the integrated-pressure data and the force-balance data were obtained. In

this paper, the lift and pitching moment data reported for the clean configuration were obtained from the surface pressures while the data reported for the iced configurations were obtained from the force balance. In many cases, the stall of the iced-airfoil configurations was characterized by unsteady flow. The available signal conditioning for the force-balance data allowed for more effective filtering of these unsteady effects. Drag coefficient was calculated from the wake pressures using standard momentum-deficit methods and these values are reported in this paper for all configurations. The performance coefficients were corrected for wind-tunnel wall effects using the methods of Allen and Vincenti.[20] The angle of attack sweeps were performed for a large range of Reynolds numbers and Mach numbers as shown in Table 1. The matrix was designed to isolate the independent effects of these parameters. Therefore, Reynolds numbers variations were performed at constant Mach numbers of 0.10 and 0.20 while a Mach number variation was performed at a constant nominal Reynolds number of 12×10^6. The Reynolds number was not maintained entirely constant for each of these conditions, and therefore Table 1 indicates the variation over the course of the entire test campaign.

Table 1 Matrix of Reynolds and Mach Number Conditions.

	Mach Number		
Reynolds Number Range	0.10	0.20	0.28
4.5×10^6 to 4.6×10^6	X		
8.0×10^6 to 9.1×10^6	X	X	
12.0×10^6 to 12.3×10^6	X	X	X
15.8×10^6 to 16.0×10^6		X	

A total of six ice accretion simulations were tested. Using the ice accretion classifications developed by Bragg et al.[5,6] there was one horn shape, one spanwise-ridge shape, two roughness shapes and two streamwise shapes. The casting simulations were fabricated from ice accretion moldings acquired during an earlier campaign in the NASA Glenn Icing Research Tunnel (IRT). This testing and methodology is described in more detail by Bragg et al.[4] Table 2 summarizes the icing conditions associated with the ice accretions selected for aerodynamic testing. These ice accretions are documented in Figs. 2-7. The horn shape in Fig. 2 shows the classic upper-surface horn typical of this glaze-type accretion. The streamwise shape in Fig. 3 is more conformal to the leading-edge radius with a smooth zone on the nose followed by downstream rime feather roughness. The glaze roughness in Fig. 4 had a smooth zone in the stagnation region followed by large roughness downstream. The spanwise-ridge shape in Fig. 5 was formed by applying a heater mat to the model leading edge. The heat input and icing conditions were adjusted to accrete the upper and lower surface ridges shown in Fig. 5. The streamwise shape in Fig. 6 was selected for aerodynamic testing because it had a more "pointed" geometry at the leading edge and was less conformal to the surface than the other streamwise shape (Fig. 3). The remaining roughness case in Fig. 7 was formed in cold conditions resulting in very fine rime feathers that were very different in size and distribution from the glaze roughness case in Fig. 4.

Table 2 The Ice Accretions Selected for Aerodynamic Testing.

Ice Classification	Run No.	Airspeed knots	AoA deg.	MVD μm	LWC g/m^3	Total Temp. F/C	Static Temp. F/C	Spray Time min.
Horn	EG1164	175	5.0	20	0.85	28.0/-2.2	20.8/-6.2	11.3
Streamwise #1	EG1162	150	2.0	30	0.55	-8.0/-22.2	-13.5/-25.3	10.0
Roughness #1	EG1126	200	2.0	20	0.50	28.0/-2.2	18.6/-7.4	2.0
Spanwise Ridge	EG1159	150	1.5	20	0.81	20.0/-6.7	14.8/-9.6	15.0
Streamwise #2	EG1125	200	2.0	15	0.30	4.0/-15.6	-5.3/-20.7	20.0
Roughness #2	EG1134	200	2.0	40	0.55	4.0/-15.6	-5.3/-20.7	2.0

For each ice accretion a set of casting simulations were fabricated for aerodynamic testing. The castings were made from a hard two-part polyurethane-type material of very low viscosity required to flow into the intricate details of the ice molds. The moldings of the ice accretions were limited to a span of 15-inches (381-mm) at the center of the IRT model. This was of sufficient length to reproduce the spanwise variation in all of the ice accretion geometries. Therefore, multiple sections of casting were fabricated for each ice shape to cover the 137.48-inch (3492-mm) span of the NACA 23012 model. A total of 10 sections were used, each having a finished length of 13.75-inches (349.3-mm). The sections were bolted on to the alternate leading edge of the model and the interfaces

were sealed with caulk. A completed installation is shown in Fig. 8. One casting section was instrumented with static pressure taps. This was located at the same spanwise station as the main chordwise row on the model (43% span measured from the test-section floor). The orifices were drilled directly into the casting and located in areas conducive to good surface static pressure measurements based upon previous research.[7] The number of pressure taps on the entire removable section ranged from 29 to 36 with some ice shapes requiring higher resolution. The pressure orifice locations are indicated in the tracings of Figs. 2-7. These tracings were obtained from the casting of the ice shape instead of from the tunnel ice accretion.
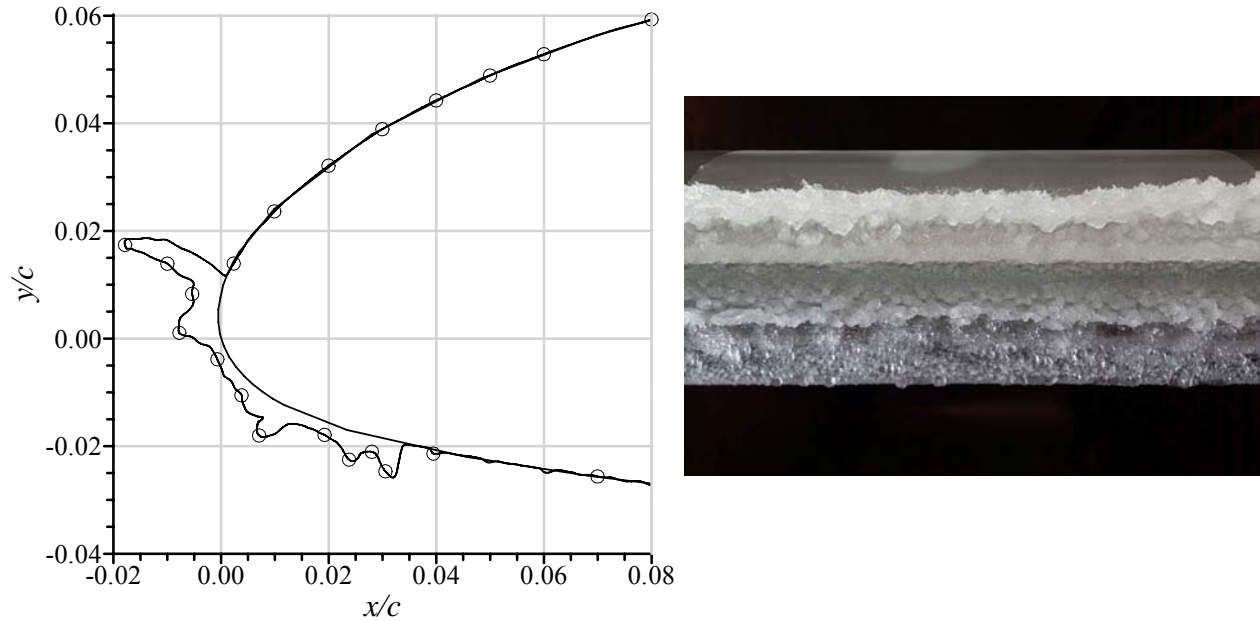
Fig. 2 Tracing and photograph of horn shape EG1164. Tracing taken from ice casting used for aerodynamic testing with pressure orifice locations indicated by open circles.
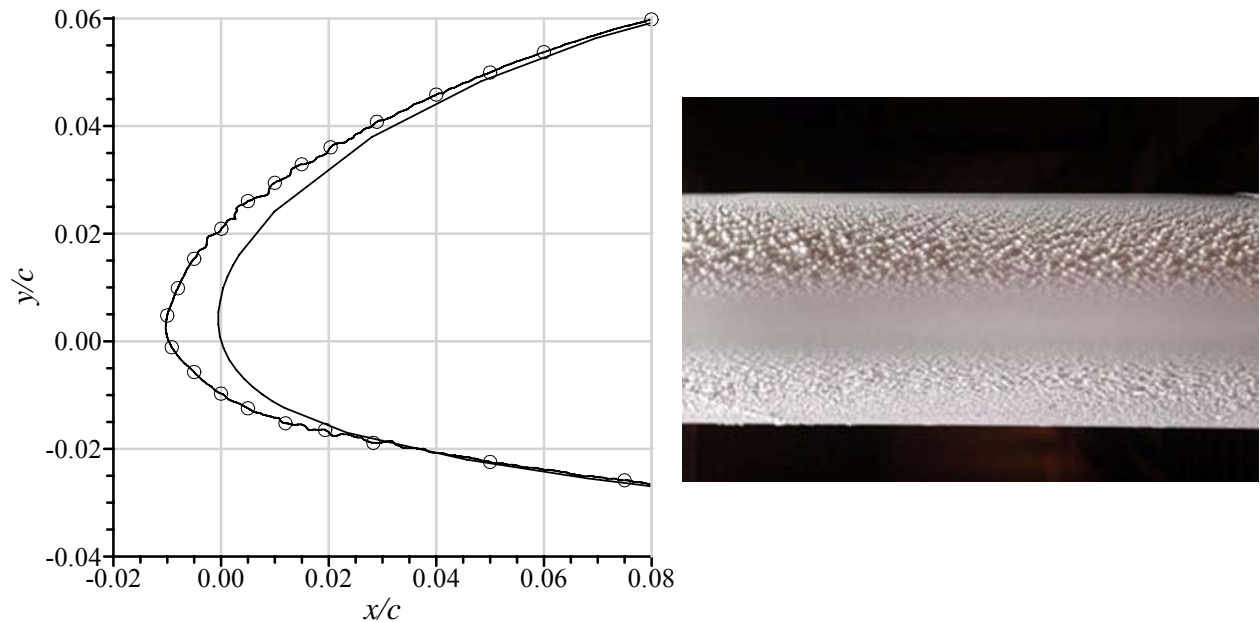
Fig. 3 Tracing and photograph of streamwise shape #1 EG1162. Tracing taken from ice casting used for aerodynamic testing with pressure orifice locations indicated by open circles.
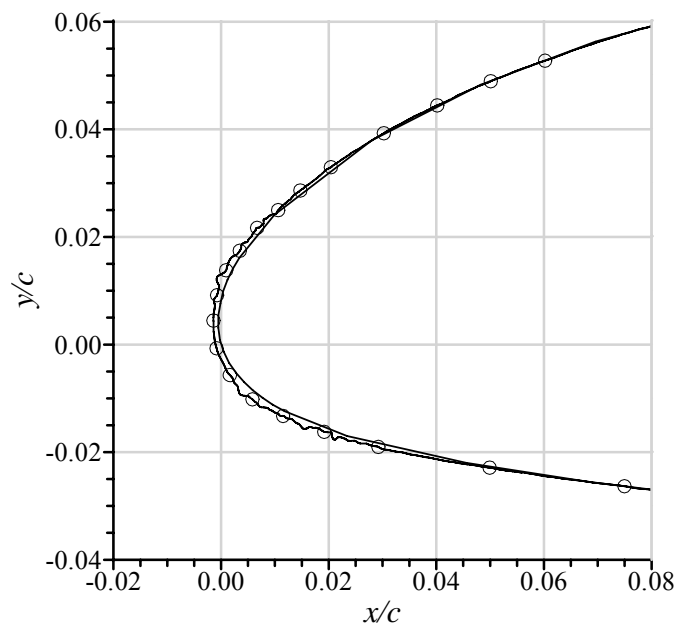
Fig. 4 Tracing and photograph of roughness shape #1 EG1126. Tracing taken from ice casting used for aerodynamic testing with pressure orifice locations indicated by open circles.
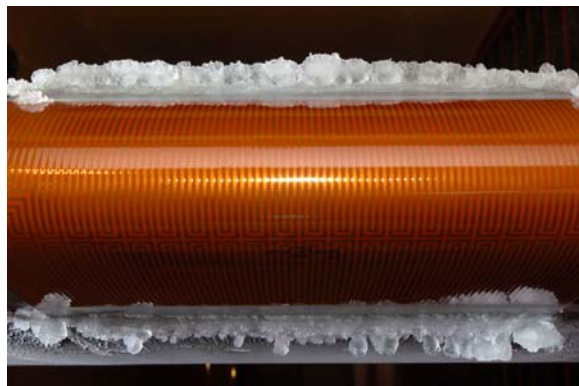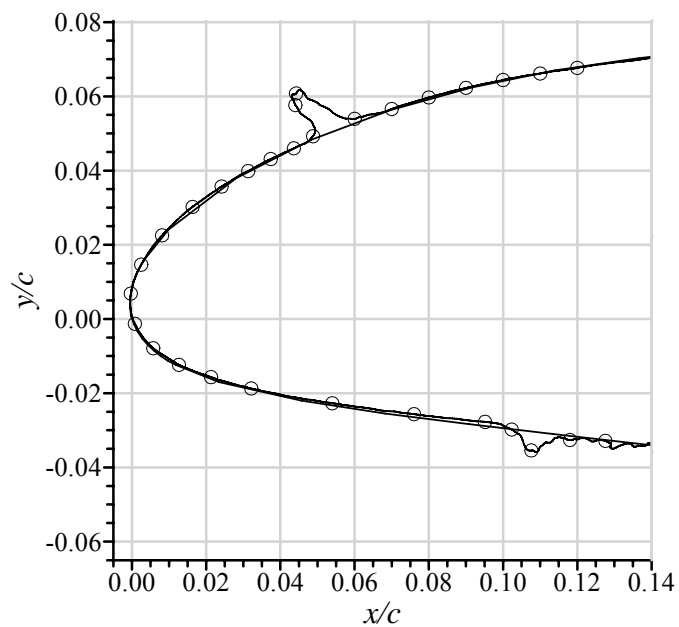
Fig. 5 Tracing and photograph of spanwise-ridge shape EG1159. Tracing taken from ice casting used for aerodynamic testing with pressure orifice locations indicated by open circles.

American Institute of Aeronautics and Astronautics
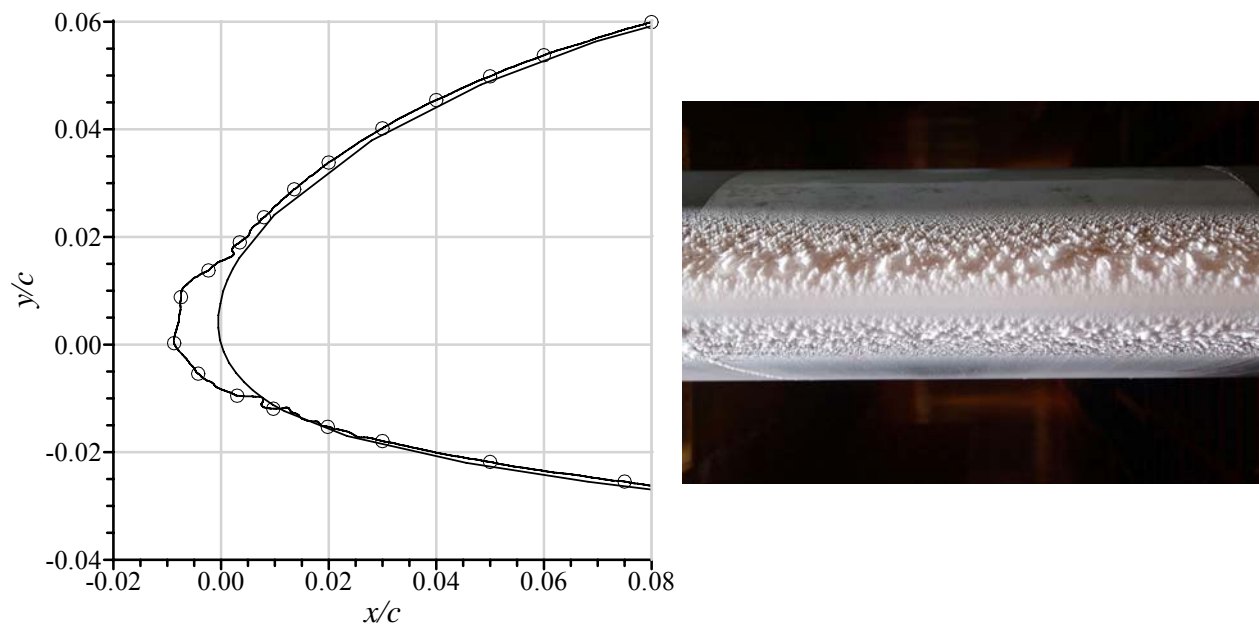
Fig. 6 Tracing and photograph of streamwise shape #2 EG1125. Tracing taken from ice casting used for aerodynamic testing with pressure orifice locations indicated by open circles.
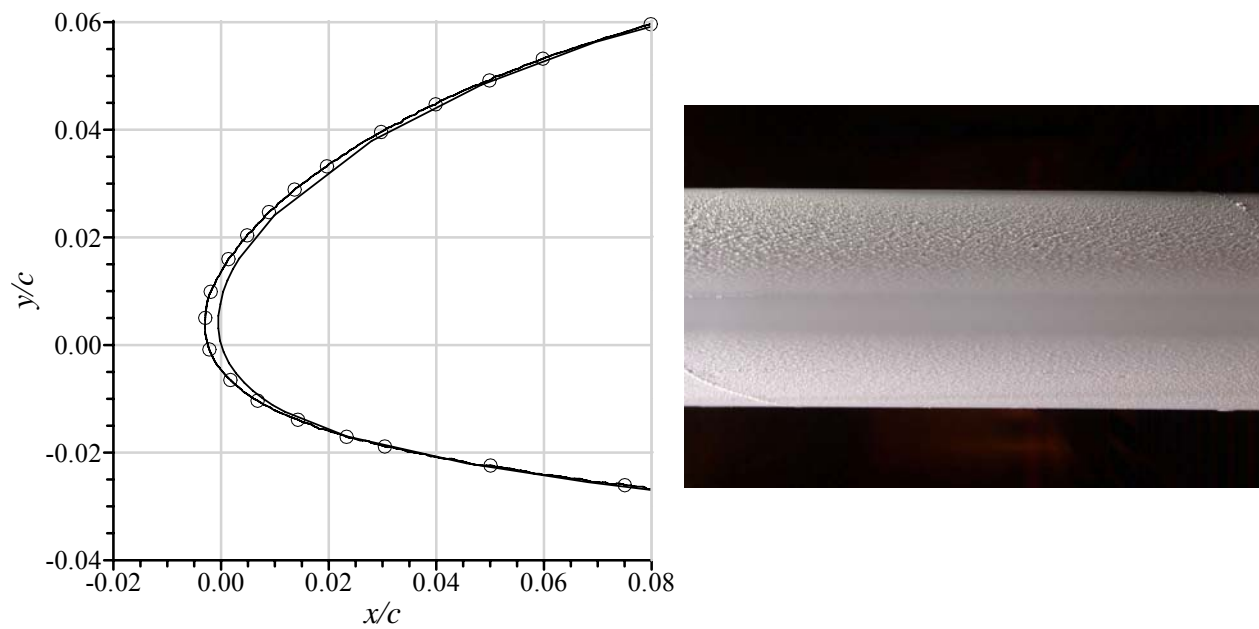
Fig. 7 Tracing and photograph of roughness shape #2 EG1134. Tracing taken from ice casting used for aerodynamic testing with pressure orifice locations indicated by open circles.

American Institute of Aeronautics and Astronautics

Fig. 8 Completed installation of horn shape EG1164 casting sections on the leading edge of the NACA 23012 airfoil model (upper-surface view).

III. Results and Discussion

A. Clean Airfoil Aerodynamics

The NACA 23012 airfoil model was tested in the baseline configuration to establish the clean performance over the given range of Reynolds and Mach numbers. Overall, the clean-airfoil results followed classic airfoil behavior and compared favorably with existing data. Validation of the clean performance was established primarily by comparison of the present data with archival data and XFOIL results for the NACA 23012 airfoil section. An example of this comparison is shown in Fig. 9 for approximately matched Reynolds and Mach number conditions. Two sets of historical data were available. The first, Broeren et al.,[13] was a more recent test of a 36-inch chord NACA 23012 airfoil in the NASA Langley Low-Turbulence Pressure Tunnel (LTPT) at $Re = 7.5 \times 10^6$ and $M = 0.21$. The second is the historical data of Abbott and von Doenhoff[21] who tested a 24-inch chord NACA 23012 airfoil also at LTPT. These data are for $Re = 8.8 \times 10^6$ and $M < 0.17$ (the exact Mach number was not given). The lift coefficient versus angle of attack trend shows very good agreement. The Broeren et al.[13] data had a slightly higher slope for angles of attack preceding the stall, while the Abbott and von Doenhoff data had a slightly lower slope for negative angles of attack. The sharp stall of the clean airfoil is indicative of leading-edge stall. For this stall type, laminar separation occurs near the leading edge without subsequent reattachment, resulting in separated flow over the airfoil and the significant decrease in lift.[22] The agreement in maximum lift coefficient was very good and well within the range of experimental uncertainty and potential variations in wall-correction methods. The present data had $C_{l,max} = 1.82$ while the values for Broeren et al.[13] and Abbott and von Doenhoff[21] were 1.81 and 1.80, respectively. There was a slightly larger discrepancy in stalling angle of attack with $\alpha_{stall} = 18.1$ deg. for the present data and 17.6 deg. and 18.4 deg. for the archival sources. Some of this disagreement could be due to the angle of attack resolution at which the data were acquired. For example, the Broeren et al.[13] data were only acquired in one degree increments, so it is quite possible that a higher stalling angle could have been measured with finer resolution in that test. The XFOIL results were computed for a Reynolds number of 9.0×10^6 and a Mach number of 0.20. XFOIL is an airfoil analysis code that couples a panel method flowfield solver to an integral boundary-layer formulation.[23] The lift coefficient trends show that the XFOIL results compared favorably with the all of the experimental data. The former had a slightly higher lift-curve slope which is a common characteristic of XFOIL results, in the authors' experience.

The agreement in the quarter-chord pitching moment variation with angle of attack was very good between the present data and the Broeren et al.[13] data, with the latter being slightly more nose down for positive angles of attack. The agreement with the Abbott and von Doenhoff[21] pitching-moment data is not as good owing to some noted deficiencies due to their balance arrangement.[13,21] The XFOIL calculations also reproduce the appropriate C_m vs. α trend, matching up best with the Broeren et al.[13] data. For drag coefficient, the agreement between the present data

and Abbott and von Doenhoff[21] is good, particularly for lift coefficients less than about 1.0. Both data sets have the characteristic reduction in C_d at $C_l \approx 0.10$, also present in the XFOIL results. The large difference in the Broeren et al.[13] C_d data was shown to be related to the mismatch of spanwise running seams for the removable leading edge on that model. While the present model also had a removable leading edge, the match of the spanwise running seams was excellent. The Abbott and von Doenhoff[21] model was solid, i.e., no seams. The XFOIL results agreed fairly well with the present data and Abbott and von Doenhoff for most of the lift range until $C_l \approx 1.0$. These performance comparisons show that valid data were obtained for the clean NACA 23012 airfoil section in the current work.
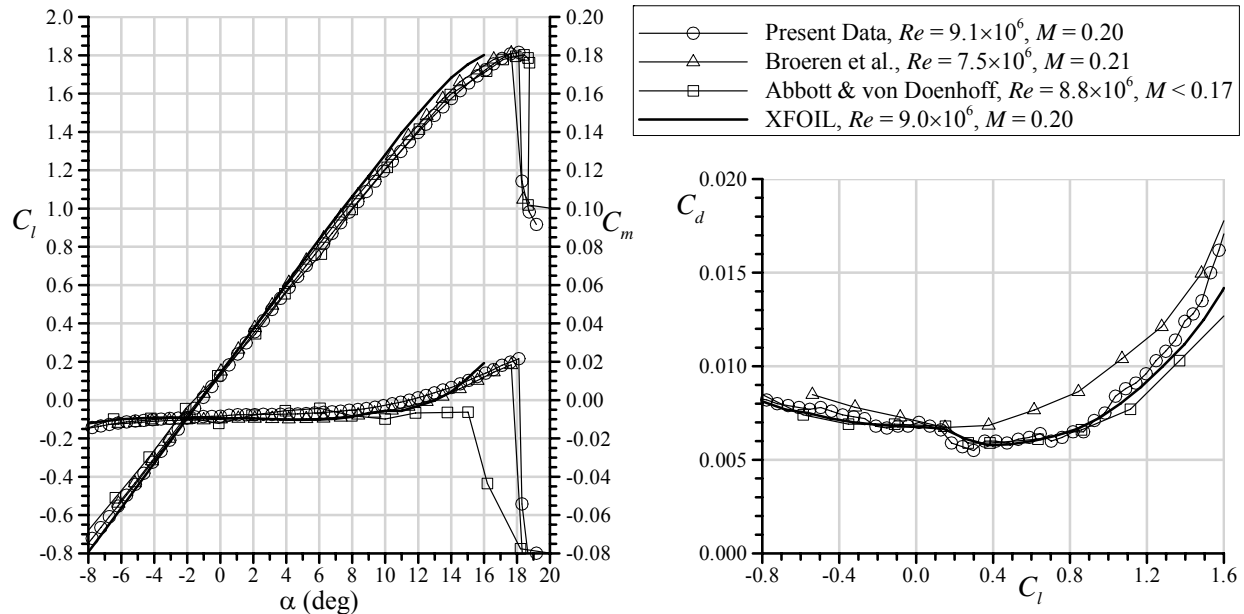
Fig. 9 Comparison of clean NACA 23012 airfoil section performance from the current work with results from Broeren et al.,[13] Abbott and von Doenhoff[21] and XFOIL at closely matched Reynolds and Mach number.

The pressurization capability of the F1 facility allowed for the independent exploration of Reynolds and Mach number effects on the airfoil performance. The performance results for the NACA 23012 exhibited classic airfoil behavior. For example, the lift data show that $C_{l,max}$ increased from 1.76 at $Re = 4.6 \times 10^6$ to 1.84 at $Re = 8.1 \times 10^6$ to 1.88 at $Re = 12.3 \times 10^6$ with $M = 0.10$. The stalling angle also increased over this range of Reynolds number and the pitching moment values near stall also became slightly more nose down. These Reynolds number trends agree with archival data for the NACA 23012 and data for other airfoils. The effect on maximum lift coefficient is summarized in Fig. 10. Included in Fig. 10 are NACA 23012 section data from Abbott and von Doenhoff,[21] NACA 0012 data reported by Ladson[24] and GLC-305 data from Addy et al.[14] The NACA 0012 data were acquired in the NASA Langley LTPT on a 24-inch chord model. The GLC-305 data were also acquired in the LTPT using a 36-inch chord model. This airfoil section was fairly thin (less than 9%) and not highly cambered, thus resulting in the lower $C_{l,max}$ values shown in Fig. 10. These data indicate that large increases in $C_{l,max}$ occur for Reynolds numbers less than about 6.0×10^6 and increasing Reynolds number above this results in only modest increases in $C_{l,max}$. There is good agreement in the $C_{l,max}$ values for the three different sources of the NACA 23012 section data in Fig. 10, especially given the difference in models, facilities and installations. Some of the difference can also be attributed to differences in Mach number.

The effects of compressibility were documented for the clean NACA 23012 airfoil section by varying Mach number from 0.10 to 0.28 at a constant Reynolds number of 12.1×10^6. Once again, classic airfoil behavior was observed in the characteristic increases in the lift-curve slope and pitching-moment slope just prior to stall for increasing Mach number. The maximum lift coefficient and stalling angle of attack both decreased with increasing Mach number, as expected. These results for $C_{l,max}$ are summarized in Fig. 11 along with data from the other sources mentioned in connection with Fig. 10. The data for the NACA 0012 and GLC-305 airfoils show more

significant reduction in $C_{l,max}$ for Mach numbers larger than 0.20, while the data for the NACA 23012 section show mixed results. The present data indicate a more linear decrease in $C_{l,max}$ over the given Mach number range, while the trend in the Broeren et al.[13] data aligns more closely with the other airfoils. Despite these minor differences, the overall Reynolds and Mach number effects and the comparison to historical data yield confidence in these measurements.
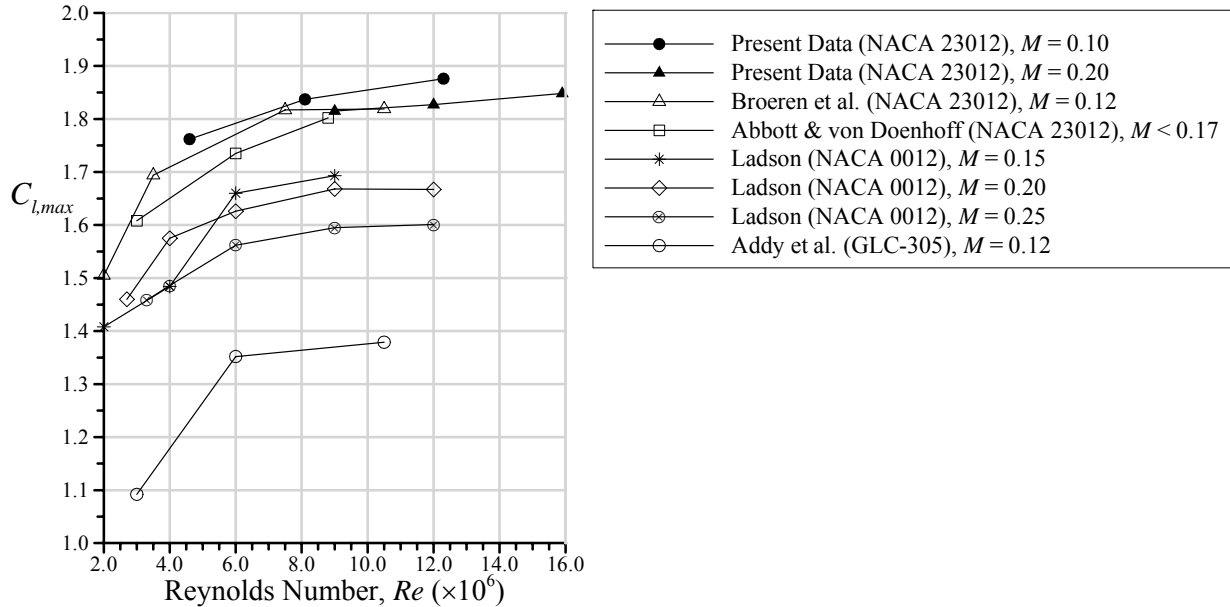
Fig. 10 Comparison of the effect of Reynolds number on maximum lift coefficient for the NACA 23012 airfoil from the current work, Broeren et al.[13] and Abbott and von Doenhoff[21] with the NACA 0012 airfoil from Ladson[24] and with the GLC-305 airfoil from Addy et al.[14]
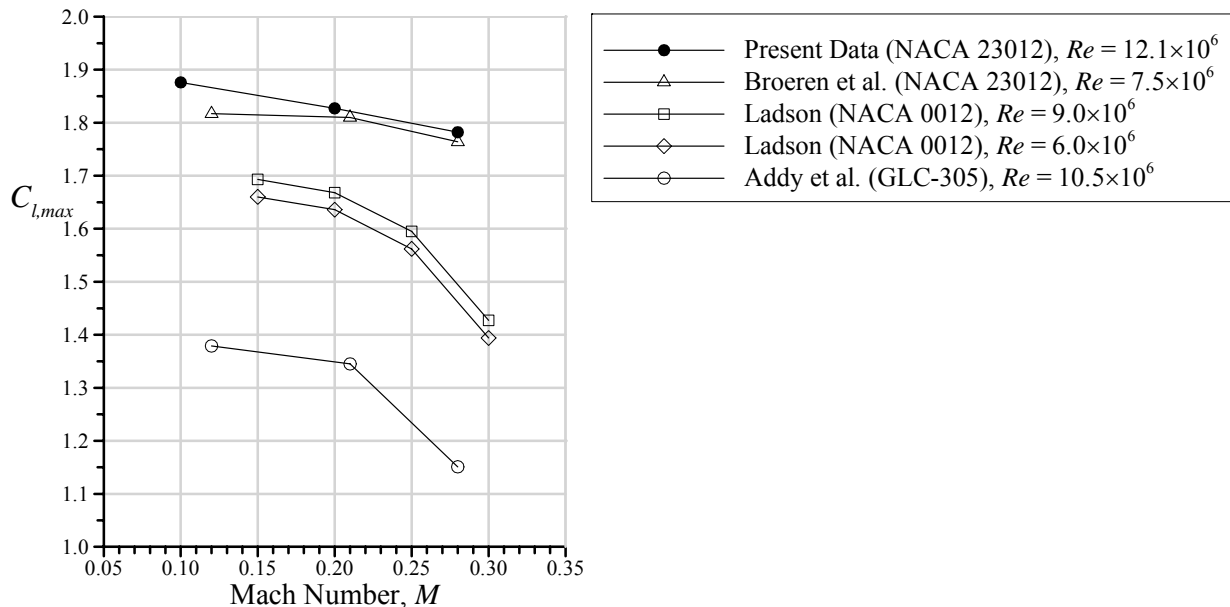
Fig. 11 Comparison of the effect of Mach number on maximum lift coefficient for the NACA 23012 airfoil from the current work with data from Broeren et al.[13] and with the NACA 0012 airfoil from Ladson[24] and the GLC-305 airfoil from Addy et al.[14]

B. Iced-Airfoil Aerodynamics

The ice casting simulations applied to the NACA 23012 airfoil caused a large range of detrimental performance effects due to the differences in the ice accretion geometries and roughness levels. The general range in performance degradation is illustrated in Fig. 12 for four of the six artificial ice shapes at $Re = 15.9 \times 10^6$ and $M = 0.20$. The clean airfoil $C_{l,max}$ value was 1.85 and α_{stall} was 18.1 deg. for this Reynolds and Mach number condition. The EG1162 streamwise and EG1126 roughness shapes had a very similar effect on lift, drag and pitching moment. The effect of the EG1162 ice simulation was to reduce $C_{l,max}$ to 1.16 and α_{stall} to 11.9 deg. The EG1126 roughness shape caused a slightly larger lift penalty, yielding $C_{l,max} = 1.09$ at $\alpha_{stall} = 11.4$ deg. Both of these ice simulations caused a significant redistribution of surface pressure resulting in an increase in the pitching-moment slope. The stall characteristics and surface pressure distribution indicate that there was likely some boundary-layer separation on the aft portions of the airfoil ("trailing-edge separation"). Yet the sharp drop in C_l near $C_{l,max}$ is reminiscent of the clean leading-edge stall type. The plot of drag coefficient shows that the EG1162 and EG1126 shapes also had a similar effect, with the former having a slightly higher C_d up to $\alpha \approx 8.5$ deg., where there was a crossover. At higher angles of attack the EG1162 streamwise ice shape caused a lower C_d, which is consistent with the higher lift coefficients.

The performance results with the streamwise (EG1162) and roughness (EG1126) shapes sharply contrast the effect of the horn (EG1164) and spanwise-ridge (EG1159) shapes. The size and location of the latter two ice shapes on the airfoil caused large upper-surface separation bubbles that significantly altered the flowfield and the subsequent performance. The resulting maximum lift coefficient for the EG1164 horn shape was 0.86 at $\alpha_{stall} = 8.8$ deg. which amounted to a 54% reduction in $C_{l,max}$ from the clean airfoil at this Reynolds and Mach number condition. The effect of the EG1159 spanwise-ridge shape was even more severe with $C_{l,max} = 0.52$ at $\alpha_{stall} = 5.6$ deg. The lift and pitching moment data for the airfoil with these ice shapes are consistent with the understanding of the flowfield effects relating to the large separation bubble formed downstream of the horn and ridge.[5,6] The upper-surface separation bubble grows with increasing angle of attack until the reattachment region reaches the airfoil trailing edge. These are the essential features of the classic thin-airfoil stall type described in detail by McCullough and Gault.[22] The plot of drag coefficient in Fig. 12 further illustrates the significant impact of the separation bubble for the EG1164 and EG1159 ice-shape simulations. It is interesting to note that C_d for the EG1159 spanwise ridge is lower than that for the EG1164 horn shape for angles of attack less than about -2.5 deg. This most likely occurred because at low angle of attack drag coefficient is affected primarily by ice accretion on the airfoil lower surface. A comparison of Figs. 2 and 5 clearly shows that the horn shape had larger height and extent of ice accretion on the lower surface, albeit closer to the leading edge. This effect of lower and upper-surface ice accretion on drag is
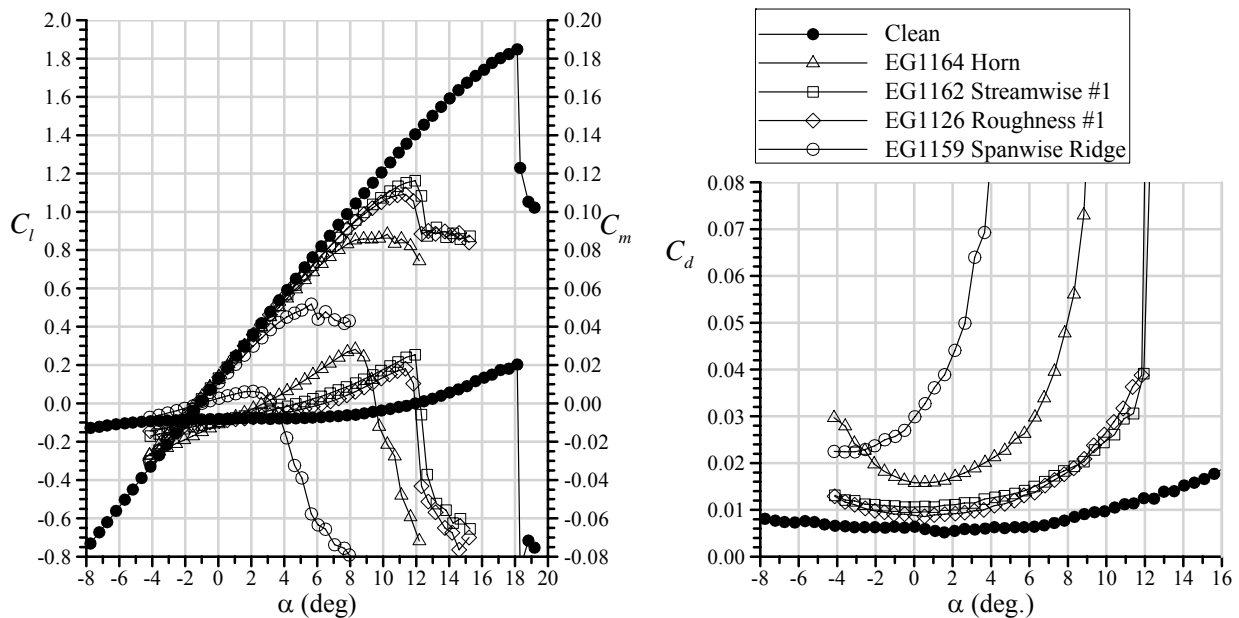
Fig. 12 Comparison of performance effects of the simulated ice configurations on the NACA 23012 airfoil at $Re = 15.9 \times 10^6$ and $M = 0.20$.

described by Bragg et al.[6] and in much more detail by Kim.[25] For angles of attack larger than -2.5 deg., the drag coefficient for the spanwise-ridge shape was much larger, which was consistent with the lower $C_{l,max}$. The fact that the spanwise-ridge ice simulation resulted in the largest performance degradation was likely due to the location of the upper-surface ridge. As depicted in Figs. 2 and 5, the horn height was larger than the upper-surface ridge, but the ridge was located at $x/c \approx 0.06$. Lee et al.[26] showed that for the NACA 23012 airfoil, the most sensitive location for ice accretion (of this size) in terms of loss in maximum lift was downstream of the leading edge. This is also illustrated in Fig. 12 for the streamwise shape that formed on the airfoil leading edge, as the performance penalty was not nearly as severe as for the spanwise ridge.

The effect of leading-edge ice accretion on the NACA 23012 airfoil performance is further illustrated in Fig. 13. These data are for the EG1125 and EG1134 streamwise and roughness ice shapes compared to the streamwise and roughness shapes plotted in Fig. 12. Of these, it is interesting to note that the lowest iced-airfoil $C_{l,max}$ occurred with the EG1126 roughness shape. The drag penalty was also largest for this shape for angles of attack greater than 9 deg. The fact that the two streamwise ice simulations (EG1162 and EG1125) had a nearly identical effect on $C_{l,max}$ and C_d (for $\alpha > 9$ deg.) as the EG1126 roughness shape reveals an important characteristic about leading-edge ice accretion on the NACA23012 section. A comparison of the ice accretion characteristics in Figs. 3, 4 and 6 and icing environment in Table 2, shows a wide range of icing conditions and resulting sizes and shapes. The obvious implication is that the basic ice height or thickness for these types of accretions is not a strong driver of the stall performance behavior. A similar effect has been observed in previous testing of a subscale NACA 23012 airfoil with larger geometric quarter-round ice simulations located at the leading edge (i.e., $x/c = y/c = 0$). Lee and Bragg[26] showed that the iced airfoil $C_{l,max}$ varied from about 1.01 to 0.97 as the ice height (or thickness) varied from $k/c = 0.014$ to 0.006. A similar $C_{l,max}$ range was observed in Fig. 13; 1.09 for the EG1126 simulation to 1.16 for the EG1162 simulation. Despite the similarity in $C_{l,max}$ values, there is a difference in the stalling characteristics with the EG1162 and EG1126 simulations having a sharper, leading-edge type stall versus the EG1125 simulation that resulted in a more gradual trailing-edge type stall. This implies that significant flowfield differences remain among the various artificial ice shapes despite the alignment of maximum lift coefficient. These effects are addressed further in subsection D.

The data for the EG1134 simulation illustrate the smallest maximum lift penalty measured for the given set of artificial ice shapes. The $C_{l,max}$ of 1.28 was about 10% higher than for the other three ice simulations in Fig. 13. The drag coefficient on the interval $-1.5 < \alpha < 4.7$ deg. was slightly higher than, but most similar to the drag coefficient for the other roughness simulation, EG1126. It is interesting that the lift performance of the NACA 23012 section with the EG1134 simulation was very similar to the 80-grit sandpaper ($k/c = 0.00023$) reported by Broeren et al.[13] on the 36-inch chord model of the same airfoil. For that case, the $C_{l,max}$ was about 1.30 at $Re = 7.5 \times 10^6$ and $M = 0.21$.
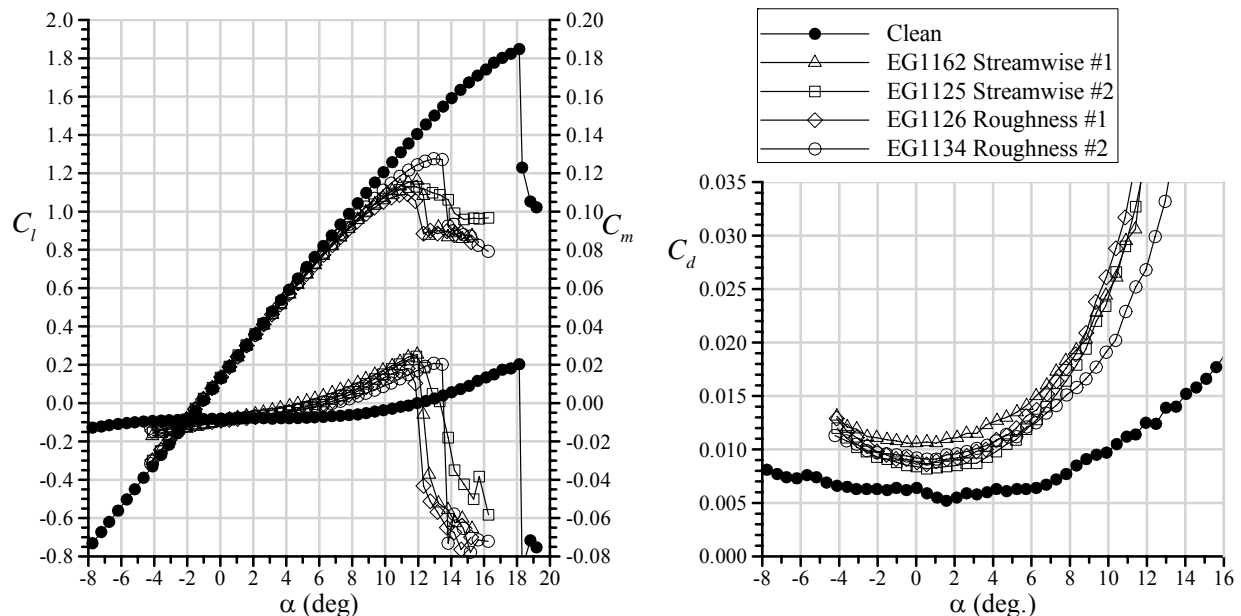
Fig. 13 Comparison of performance effects of the roughness and streamwise ice simulations on the NACA 23012 airfoil at $Re = 15.9 \times 10^6$ and $M = 0.20$.

The minimum C_d for the airfoil with the 80-grit sandpaper was 0.010, about 10% higher than for the EG1134 roughness simulation in the present data. The comparison of the EG1134 performance effects to the 80-grit sandpaper on the 36-inch chord model is useful because the latter is roughly equivalent to 40-grit sandpaper on a full-scale wing, which is often used in aircraft certification flight testing applications.[27]

The trends in the drag coefficient variation with angle of attack for the iced-airfoil configurations in Fig. 13 may be interpreted in terms of the icing environment from which these simulations were obtained. In the case of the two streamwise ice simulations, for example, the drag coefficient for the EG1162 configuration was higher than for the EG1125 configuration in the range of -4 to 8 deg. This is somewhat surprising given that the former ice shape was more conformal to the airfoil leading edge than the latter. However, the former was accreted with a larger MVD drop size and therefore the downstream roughness covered a larger surface extent. This may be at least partially responsible for the larger drag over this range. It was noted above that the drag coefficient for the EG1134 roughness configuration was slightly higher than for the EG1126 roughness configuration over the interval $-1.5 < \alpha < 4.7$ deg. This may have occurred because the rime roughness EG1134 was accreted with a larger drop size resulting in a larger surface extent of ice roughness. For angles of attack larger than 4.7 deg., it was likely that a larger extent of trailing-edge separation developed for the EG1126 configuration, thus the drag coefficient grew larger than for the EG1134 configuration corresponding to the lower stalling angle.

C. Iced-Airfoil Reynolds and Mach Number Effects

The effect of Reynolds number variation at constant Mach number is shown in Fig. 14 for the EG1125 streamwise-ice simulation. The lift and pitching moment data remain virtually unchanged despite a nearly three-fold increase in Reynolds number from 4.6×10^6 to 12.0×10^6. There was a small increase in maximum lift coefficient from 1.10 at the lowest Reynolds number to 1.13 at the highest. The pitching moment data show that there was a small 0.5 deg. increase in the stall break as the Reynolds number was increased from 4.6×10^6 to 8.2×10^6. The drag data show slightly more dependence with the drag coefficient generally decreasing with increasing Reynolds number. The reason for this trend was not investigated in detail, but this effect on drag has been observed in other iced-airfoil studies.[13,14]
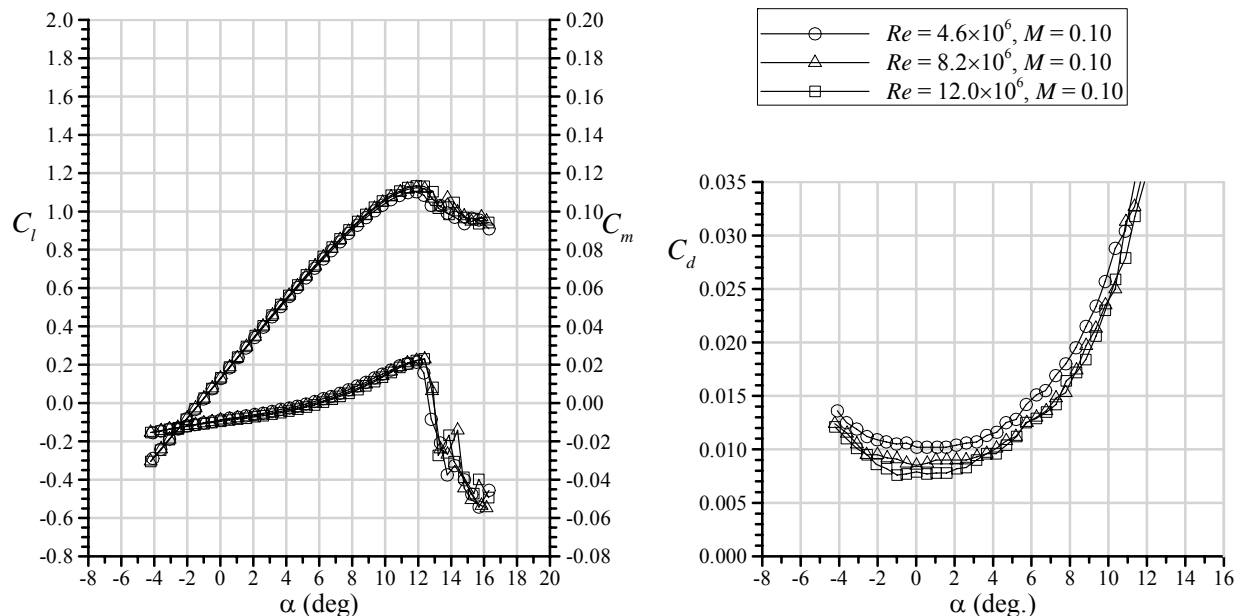
Fig. 14 Effect of Reynolds number on the performance of the NACA 23012 airfoil with the EG1125 streamwise ice simulation.

The data shown here for the EG1125 configuration was representative of all of the ice simulations tested in this study. This was particularly true for the lift and pitching moment variations with Reynolds number, even for the small roughness shapes. Changes in Reynolds number over this range did not substantially change the character of the stall either. That is, iced configurations with an abrupt, leading-edge stall character maintained this over the Reynolds number range. The effect on maximum lift coefficient for all of the simulations tested is summarized in

Fig. 15. Also included in the figure are the data for $M = 0.20$. The non-effect of Reynolds number is consistent with the previous data compiled by Bragg et al.[6] The authors argue that the presence of ice contamination on the airfoil governs the boundary-layer behavior such that the influence of Reynolds number on such processes is reduced to lower order effects unlike the clean case. The present data continue to support this conclusion.
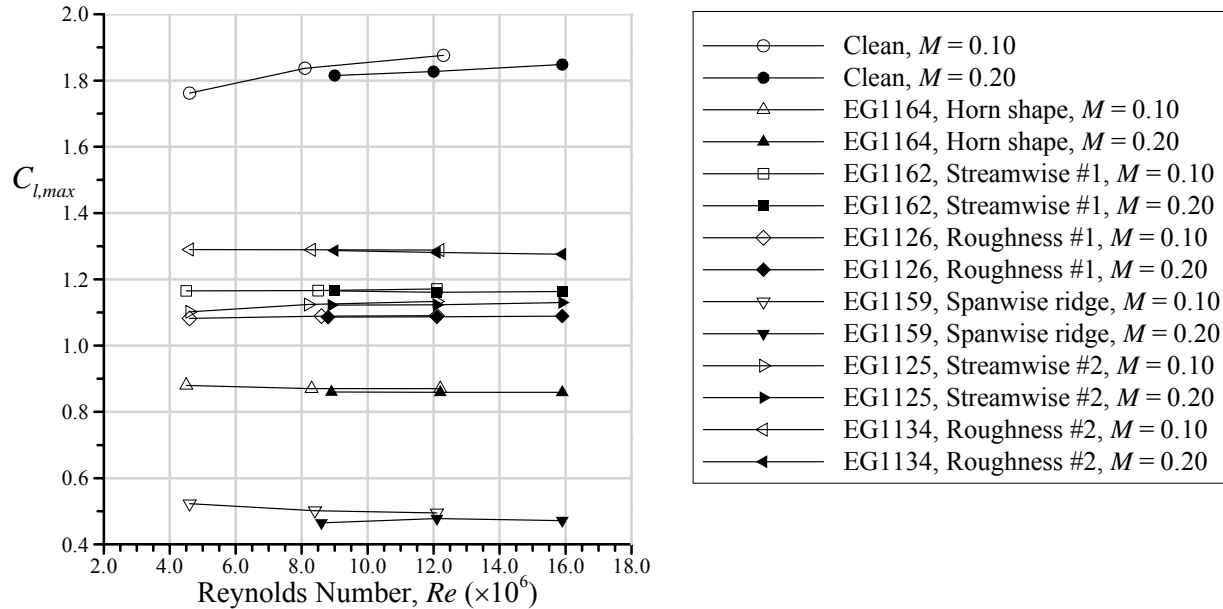
Fig. 15 Effect of Reynolds number on maximum lift coefficient for the clean NACA 23012 airfoil and with the simulated ice shapes.

The effect of Mach number variation at constant Reynolds number is shown in Fig. 16 for the same EG1125 streamwise-ice simulation. The data show that the slopes of C_l and C_m with respect to angle of attack were increased prior to stall as the Mach number was increased from 0.10 to 0.28. The maximum lift coefficient was reduced from 1.13 to 1.11 and stalling angle was reduced from 11.9 deg. to 10.9 deg. over this range. The minimum drag
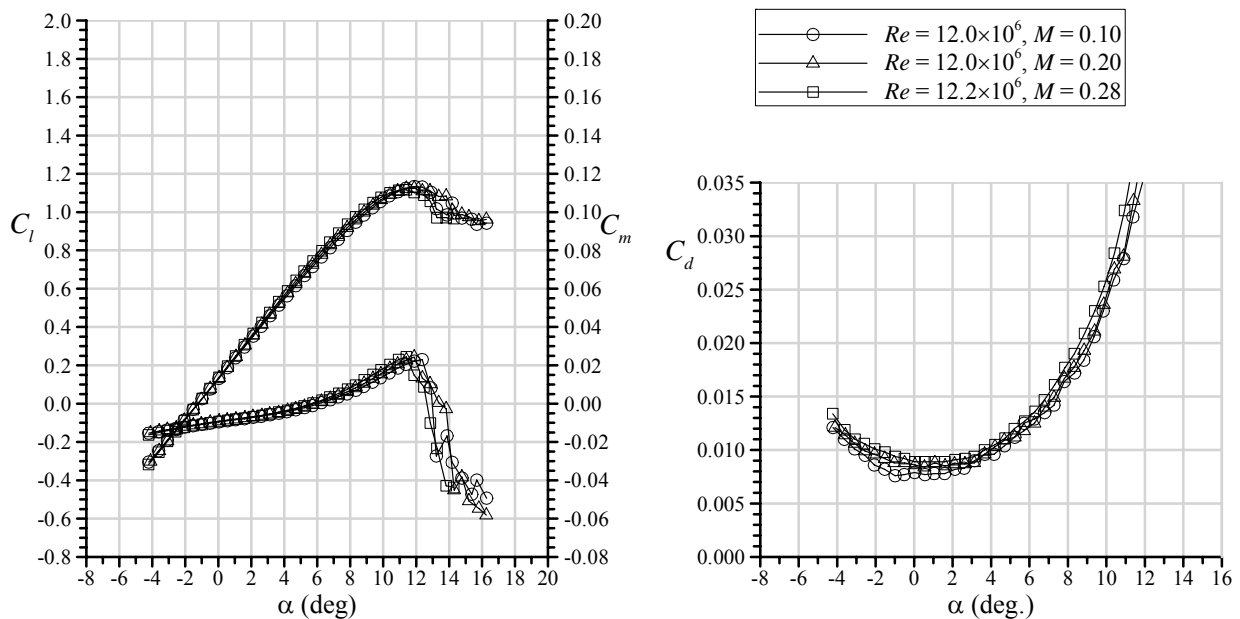
Fig. 16 Effect of Mach number on the performance of the NACA 23012 airfoil with the EG1125 streamwise-ice simulation.

coefficient increased by a larger amount for Mach number increasing from 0.10 to 0.20, with little change for Mach number increasing from 0.20 to 0.28. In contrast, drag coefficients at higher angles of attack were influenced more strongly for increasing Mach number from 0.20 to 0.28. Mach number performance sweeps for the other iced-airfoil configurations yielded similar results. The effect on maximum lift coefficient is summarized in Fig. 17. The horn shape (EG1164) and the spanwise-ridge shape (EG1159) showed the most significant decrease in $C_{l,max}$ over this range, with the smaller ice shapes showing much less dependence of $C_{l,max}$ on M. This trend involving smaller ice simulations and Mach number effects on $C_{l,max}$ has been observed in other studies. For example, Broeren et al.[13] report data for two sandpaper roughness configurations and four intercycle ice configuration on the NACA 23012 section. For the two sandpaper roughnesses, there was a very slight decrease in $C_{l,max}$ for one case and an increase in $C_{l,max}$ for the other case over a Mach number range of 0.12 to 0.28. In contrast, the much larger, ridge-type intercycle ice configurations resulted in $C_{l,max}$ variations with Mach number similar to that shown in Fig. 17 for the EG1164 and EG1159 simulations. Addy and Chung[15] performed Mach number sensitivity testing for 3-D cast ice simulations on an NLF-0414 airfoil section. The maximum lift coefficient variation for the smaller six-minute ice accretion simulation showed significantly less sensitivity to Mach number between 0.12 to 0.29 than did the larger 22.5-minute ice accretion simulation. The decrease in $C_{l,max}$ with increasing Mach number for larger ice shapes appears to be related to an increase in the size of the separated flow region and is described in more detail by Bragg et al.[6] and Broeren et al.[28]
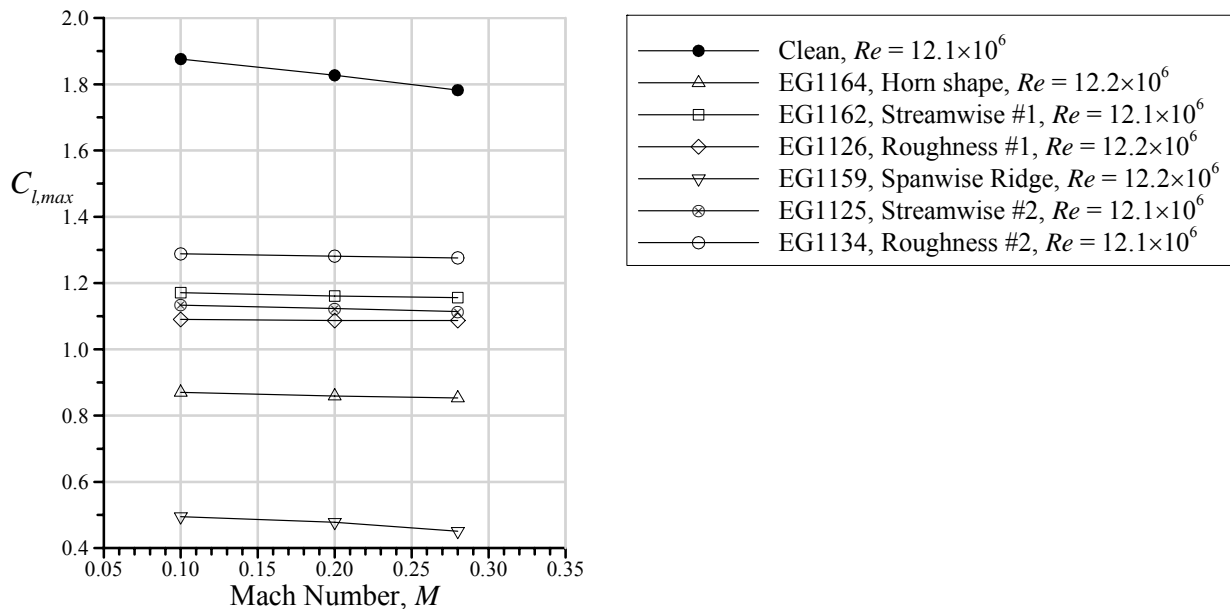
Fig. 17 Effect of Mach number on maximum lift coefficient for the clean NACA 23012 airfoil and with the simulated ice shapes.

D. Discussion of Iced-Airfoil Stalling Characteristics

The stalling characteristics of the iced-airfoil configurations tested in this study are of key interest, not only as they relate to the safety of flight operations, but also as they relate to the subscale component of this work described by Bragg et al.[4] The lack of significant Reynolds and Mach number effects on maximum lift coefficient implies that simulation of iced performance at small scale may be quite successful. In a given subscale simulation, it is also important that the stalling characteristics are maintained in addition to any one parameter such as $C_{l,max}$ or α_{stall}. Reviewing the lift performance data in Fig. 12 and the corresponding pressure distributions and flow visualization it is clear that the main stall mechanism for the EG1164 horn shape and EG1159 spanwise-ridge shape was the growth (with angle of attack) of a large upper-surface separation bubble. These flowfield physics are fairly well documented (e.g. see Bragg et al.[5,6]). However, the stalling characteristics of the streamwise and roughness ice simulations on the NACA23012 airfoil deserve a closer look. Of particular interest is that for three of these four ice simulations, the abrupt nature of the clean NACA 23012 airfoil stall was still present.

The clean NACA 23012 airfoil is classified as having leading-edge stall. The development of stall classifications relates back to early research of B. Melvill Jones,[29] among others. McCullough and Gault[22] built

upon the foundations of this early work and conducted a systematic series of airfoil section tests to establish the commonly accepted stall-type definitions in use today. They defined leading-edge stall as: "abrupt flow separation near the leading edge generally without subsequent reattachment." In their research with the NACA 63_1-012 and 63-009 airfoils exhibiting leading-edge stall, McCullough and Gault also identified the presence of a very small laminar separation bubble located just downstream of the leading edge. The authors suggested that the "bursting" of this bubble led to the abrupt flow separation and drop in lift at stall. Some years later, Tani[30] reviewed the work of McCullough and Gault in detail. Tani pointed out that the presence of the small leading-edge laminar separation bubble was dependent on Reynolds number and may not exist for Reynolds numbers larger than the 4.1×10^6 to 5.8×10^6 range of McCullough and Gault's research. However, Tani concluded that leading-edge stall could still result from laminar separation near the leading edge without subsequent reattachment. So the presence of the separation bubble prior to stall is not a necessary prerequisite for leading-edge stall. In fact, this appears to be the case for the present data on the NACA 23012 airfoil. A detailed examination of the surface pressure data at $Re = 15.9 \times 10^6$ and $M = 0.20$, showed no minor discontinuities usually associated with a laminar separation bubble. It is, of course, entirely possible that a small bubble may still have existed. Tani dubbed these as "short bubbles" precisely because they tend to have little effect on the chordwise pressure distribution. In either case, there is no question about the stall type of the clean NACA 23012 section.

What is of primary interest here is that for three of the four roughness and streamwise ice simulations tested on the NACA 23012 airfoil, the presence of the simulated ice did not appear to significantly alter the leading-edge stall type. This observation is based upon the abrupt loss in lift at stall for the EG1162, EG1126 and EG1134 simulations (cf. Fig. 13). Only the EG1125 simulation resulted in a gradual loss of lift post stall. This comparison is illustrated in more detail in the pressure distributions where the EG1134 configuration is used as the example for leading-edge stall. The data plotted in Fig. 18 for the iced-airfoil case at $\alpha = 13.5$ and 13.8 deg. show the profound redistribution of surface pressure as the stall occurs with only a 0.3 deg. increase in angle of attack. The nearly constant pressure region aft of about $x/c = 0.10$ indicated the massive separation on the upper surface indicative of the leading-edge stall type. Also shown for comparison is the clean pressure distribution for $\alpha = 13.5$ deg. At this angle of attack the clean and iced pressures were very similar. There was some divergence of the pressure near the trailing edge in the latter case indicating that there was likely some extent of turbulent boundary-layer separation. This separation combined with the effects of the ice shape probably contributed to the reduced suction pressures on the forward portion of the airfoil relative to the clean configuration. Technically, the iced-airfoil stall type may be classified as a combination of leading-edge and trailing-edge stall due to the presence of the turbulent boundary-layer separation. However, the abrupt redistribution of surface pressure is a clear hallmark of leading-edge stall.
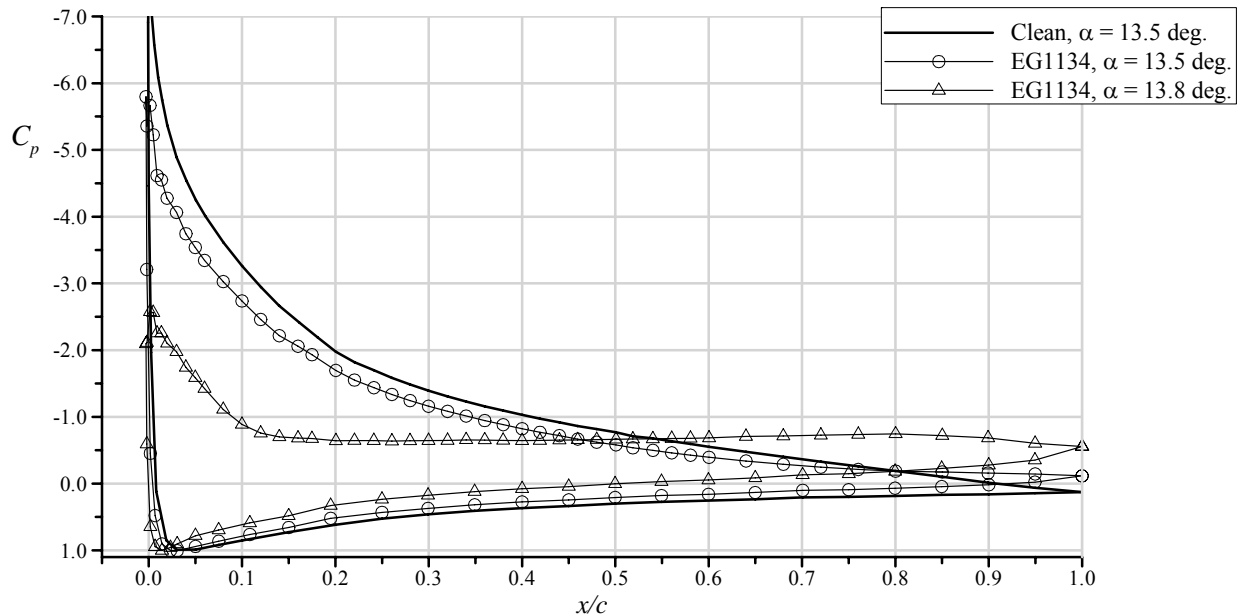
Fig. 18 Chordwise pressure distribution comparison for angles of attack near stall for the EG1134 roughness simulation on the NACA 23012 airfoil at $Re = 15.9 \times 10^6$ and $M = 0.20$.

This behavior is contrasted with the data in Fig. 19 for the EG1125 streamwise-ice simulation. The iced-airfoil pressure distributions correspond to maximum lift (α = 11.9 deg.) and 1.5 deg. post stall (α = 13.3 deg.). In contrast to the EG1134 case, the pressure distributions are comparable corresponding to the gradual reduction in lift coefficient shown in Fig. 13. There was more of a divergence of C_p on the aft section of the airfoil at the higher angle of attack indicating a larger extent of turbulent boundary-layer separation. However, the salient feature for both angles of attack is the near-constant pressure region between x/c = 0.015 and 0.05. This probably indicates the presence of a small separation bubble induced by the simulated ice shape. In this case, the bubble significantly altered the pressure distribution from the clean case, such that the tendency to leading-edge stall was altered. In fact, the EG1125 configuration could be classified as having trailing-edge stall, since the reduction in lift occurred due to the turbulent boundary-layer separation moving forward as angle of attack increased. While there was a small separation bubble present due to the ice shape, this bubble did not grow significantly in chordwise extent leading up to the stall. This partly explains the classification of this ice shape as streamwise ice, according to the descriptions established by Bragg et al.[5,6]
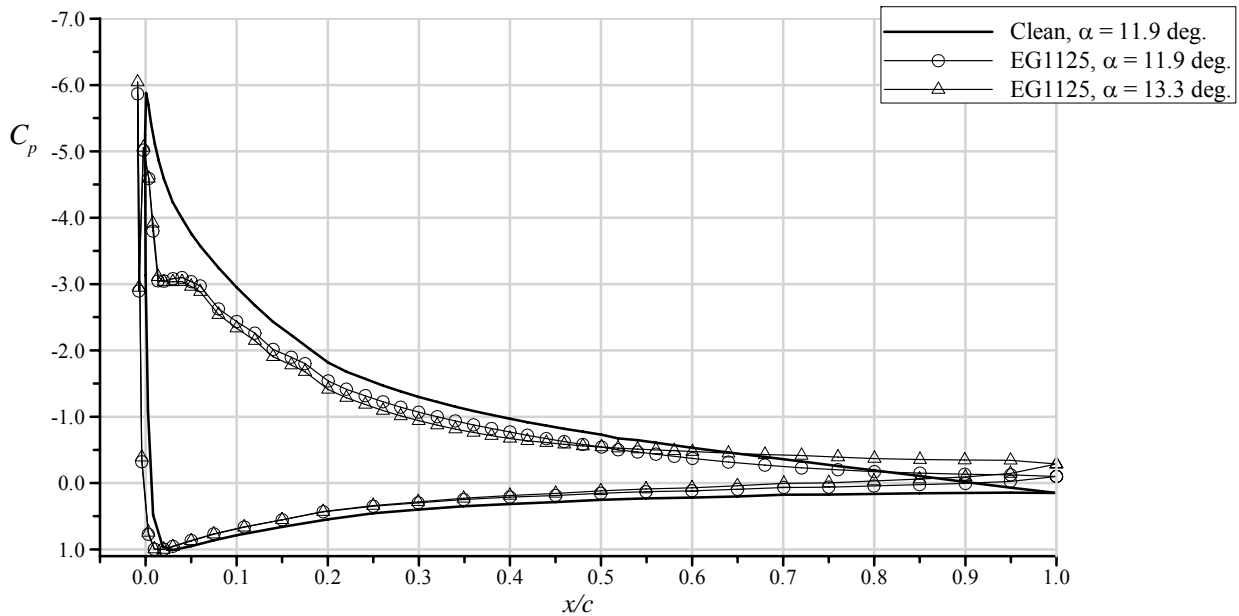
Fig. 19 Chordwise pressure distribution comparison for angles of attack near stall for the EG1125 streamwise shape on the NACA 23012 airfoil at Re = 15.9×10^{6} and M = 0.20.

The fact that the leading-edge stall characteristics of the NACA 23012 airfoil were not significantly altered by the presence of two roughness and one streamwise-ice simulations requires some explanation, albeit speculative. As mentioned in this discussion, leading-edge stall is defined as laminar separation near the leading edge of the airfoil without subsequent reattachment. With the ice simulations in question, there was likely small areas of boundary-layer separation present on the scale of the ice roughness. Research reported by Kerho and Bragg[31] showed that leading-edge roughness can lead to a "transitional" boundary layer instead of acting as a "trip" with energetic transition to turbulence. The transition process due to ice-type roughness develops over a large part of the airfoil chord, up to 30 to 50% in some cases. The present data indicate that the "transitional" nature of the boundary layer is still susceptible to abrupt separation for the three ice simulations. In contrast, the other simulations being larger, caused larger-scale separation and alteration of the transition process as well as the pressure distribution, thus leading to an alteration of the stall type.

Another important feature of the roughness and streamwise-ice simulations was that the effect on maximum lift was similar in magnitude despite the large range in geometry. As discussed in connection with Fig. 13, the range in $C_{l,max}$ was from 1.09 to 1.28. While this variation is not insignificant, it is small compared to the decrease from the clean value of 1.85. These data were compared to other results for simulated leading-edge ice contamination on the NACA 23012 airfoil shown in Fig. 20. There appears to be some dependence of $C_{l,max}$ on ice (roughness) size located at the leading edge up to $k/c \approx 0.0015$. For sizes larger than this, there is no clear trend among the data gathered from various sources. The selected data are for a large range of ice-shape geometries and simulation

methods. The roughness cases covered the leading edge, extending downstream several percent chord. The quarter-round data were simple geometric shapes with the forward face located at the leading edge. The intercycle 322 shape had characteristics similar to the EG1162 ice shape in the current study. The reduced sensitivity to these leading-edge ice simulation may be due in part to the favorable pressure gradient in this region. Since there is no clear correlation to the height of the simulated ice, the geometry, surface extent and distribution of the roughness play an important role in determining maximum lift. This type of result, while perhaps obvious in light of the present data, supports the notions of Bragg et al.[5,6] in their development of the ice-shape classifications. This leads to an ironic conclusion for subscale simulation. The reduced sensitivity may allow for lower-fidelity simulations to yield acceptable values of maximum lift coefficient. The disadvantage is that the physics of the flowfield may not be properly modeled in the subscale case. Therefore, it may actually be more difficult to develop proper subscale simulations due to the reduced performance sensitivity of the roughness and streamwise ice shapes.
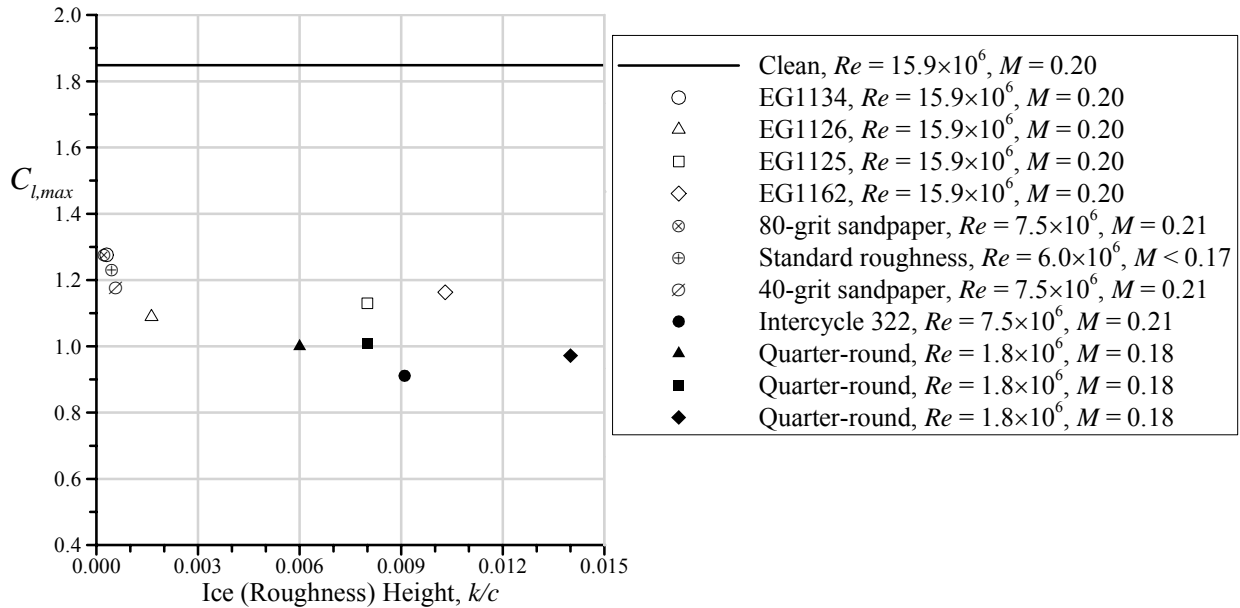
Fig. 20 Comparison of $C_{l,max}$ dependence on ice (roughness) height for various simulations all applied to the leading-edge region of the NACA 23012 airfoil. In addition to the present data, the 80-grit and 40-grit sandpaper and intercycle 322 simulations are from Broeren et al.[13] The NACA standard roughness datum is from Abbott & von Doenhoff.[21] The quarter-round data are from Lee et al.[26]

IV. Summary and Conclusions

The purpose of this paper was to report the results of a study to establish a set of high-fidelity, full-scale, iced-airfoil airfoil aerodynamic performance data. These data were acquired as a part of a larger program with the goal of developing subscale simulation methods for ice accretion. Airfoil performance testing was carried out at the ONERA F1 pressurized wind-tunnel using a 72-inch (1828.8-mm) chord NACA 23012 airfoil over a Reynolds number range of 4.5×10^6 to 16.0×10^6 and a Mach number range of 0.10 to 0.28. A total of six ice-shape simulations were tested. These simulations were high-fidelity castings made from molds obtained during earlier ice accretion testing at the NASA Glenn Icing Research Tunnel. The ice shapes were classified by their aerodynamic effect. There was one horn shape, one spanwise-ridge shape, two streamwise shapes and two roughness shapes.

The simulated ice shapes had a large detrimental effect on the performance of the NACA 23012 airfoil. The spanwise-ridge shape caused the largest reduction in maximum lift with a value of 0.52 compared to the clean value of 1.85 at $Re = 15.9\times10^6$ and $M = 0.20$. The stalling angle was also reduced from 18.1 deg. down to 5.6 deg. The minimum drag coefficient was increased by more than a factor of four from 0.0052 to 0.0224. The performance of the airfoil with the horn shape was better than with the spanwise ridge, but still severely compromised from the clean configuration. For the same Reynolds and Mach numbers, the maximum lift coefficient was 0.86 at 8.8 deg. angle of attack. The minimum drag was increased by a factor of three from the clean value. The two roughness and streamwise-ice simulations had a similar range of performance effects on the airfoil. The range of maximum lift coefficient was 1.09 to 1.28 and the range of minimum drag coefficient was 0.0082 to 0.0106 at $Re = 15.9\times10^6$ and

$M = 0.20$. The range of performance effects was small relative to the large differences in the size and geometry of the roughness and streamwise-ice shapes tested.

While the ice simulations negatively affected the stall performance of the NACA 23012 airfoil, half of the configurations tested resulted in a combination leading-edge and trailing-edge stall type. The abrupt loss of lift at stall associated with the leading-edge stall persisted for both the roughness and one streamwise-ice configurations, despite significant trailing-edge separation. This is an important detail for accurate subscale simulation because it means that while the ice shape was large enough to have a significant detrimental effect on the performance, the boundary layer in the leading-edge region was not significantly altered so as to allow separation at the leading edge without subsequent reattachment. For the remaining streamwise-ice simulation the stall type was changed to a trailing-edge stall with gradual lift loss at stall. For the horn and spanwise-ridge shapes the stall was characteristic of thin-airfoil stall since there was a large upper-surface separation bubble that grew with increasing angle of attack precipitating the stall at such low values of lift coefficient and incidence.

The pressurization capability of the ONERA F1 Facility was used to document the effects of Reynolds and Mach number on the clean and iced performance.   The clean maximum lift coefficient increased from 1.76 to 1.88 as the Reynolds number was increased from 4.6×10^6 to 12.3×10^6 at constant $M = 0.10$. Increasing Mach number from 0.10 to 0.28 at a constant $Re = 12.1 \times 10^6$ had the effect of reducing the maximum lift coefficient from 1.88 to 1.78. The trends in lift and moment slope versus angle of attack and drag coefficient were consistent with classic airfoil behavior. For the airfoil with the ice simulations, there was virtually no measurable change in maximum lift coefficient over the entire Reynolds number range tested. Changes in Mach number had minor effects on maximum lift for the horn and spanwise-ridge shapes, but virtually no effects for the others. This lack of significant Reynolds and Mach number effects implies that subscale simulation of the iced-airfoil performance may be quite successful, despite the challenges associated with the roughness and streamwise-ice configurations' stalling mechanism.

Acknowledgements

References

[1] Ratvasky, T.P., Van Zante, J.F., and Riley, J.T., "NASA/FAA Tailplane Icing Program Overview," AIAA Paper 99-0370, Jan. 1999.

[2] Ratvasky, T.P., and Van Zante, J.F., "In-Flight Aerodynamic Measurements of an Iced Horizontal Tailplane," AIAA Paper 99-0638, Jan. 1999.

[3] Ranaudo, R.J., Mikkelsen, K.L., McKnight, R.C., Ide, R.F., and Reehorst, A.L., "The Measurement of Aircraft Performance and Stability and Control After Flight Through Natural Icing Conditions," AIAA Paper 86-9758, Apr. 1986.

[4] Bragg, M.B., Broeren, A.P., Addy, H.E., Jr., Potapczuk, M., Guffond, D., and Montreuil, E., "Airfoil Ice-Accretion Aerodynamics Simulation," AIAA Paper 2007-0085, Jan. 2007.

[5] Bragg, M.B., Broeren, A.P., and Blumenthal, L.A., "Iced-Airfoil and Wing Aerodynamics," SAE Paper 2003-01-2098, Jun. 2003.

[6] Bragg, M.B., Broeren, A.P., and Blumenthal, L.A., "Iced-Airfoil Aerodynamics," *Progress in Aerospace Sciences*, Vol. 41, No. 5, Jul. 2005, pp. 323-418.

[7] Blumenthal, L.A., "Surface Pressure Measurements on a Three-Dimensional Ice Shape," M.S. Thesis, Dept. of Aerospace Eng., Univ. of Illinois, Urbana, IL, 2005.

[8] Blumenthal, L.A., Busch, G.T., Broeren, A.P., and Bragg, M.B., "Issues in Ice Accretion Aerodynamic Simulation on a Subscale Model," AIAA Paper 2006-0262, Jan. 2006.

[9] Busch, G.T., Broeren, A.P., and Bragg, M.B., "Aerodynamic Simulations of a Horn-Ice Accretion on a Subscale Model," AIAA Paper 2007-0087, Jan. 2007.

[10] Busch, G.T., "Ice Accretion Aerodynamic Simulation on a Subscale Model," M.S. Thesis, Dept. of Aerospace Eng., Univ. of Illinois, Urbana, IL, 2006.

[11] Broeren, A.P., Busch, G.T., and Bragg, M.B., "Aerodynamic Fidelity of Ice Accretion Simulation on a Subscale Model," SAE Paper 2007-01-3285, Sept. 2007.

[12] Reehorst, A.L., and Richter, G.P., "New Methods and Materials for Molding and Casting Ice Formations," NASA TM-100126, Sept. 1987.

[13] Broeren, A.P., Bragg, M.B., and Addy, H.E., Jr., "Effect of Intercycle Ice Accretions on Aerodynamic Performance," *Journal of Aircraft*, Vol. 41, No. 1, Jan.-Feb. 2004, pp 165-174.

[14] Addy, H.E., Jr., Broeren, A.P., Zoeckler, J.G., and Lee, S., "A Wind Tunnel Study of Icing Effects on a Business Jet Airfoil," AIAA Paper 2003-0727, Jan. 2003.

[15] Addy, H.E., Jr., and Chung, J.J., "A Wind Tunnel Study of Icing Effects on a Natural Laminar Flow Airfoil," AIAA Paper 2000-0095, Jan. 2000.

[16] Papdakis, M., Yeong, H.W., Chandrasekharan, R., Hinson, M., Ratvasky, T., and Giriunas, J., "Experimental Investigations of Simulated Ice Accretions on a Full-Scale T-tail," AIAA Paper 2001-0090, Jan. 2001.

[17] Addy, H.E., Jr., "Ice Accretions and Icing Effects for Modern Airfoils," NASA/TP-2000-210031, April 2000.

[18] Anderson, D.N., "Manual of Scaling Methods," NASA/CR-2004-212875, Mar. 2004.

[19] Desplas, P., "F1 Pressurized Subsonic Wind Tunnel User's Guide," Large Technical Facilities, Le-Fauga-Mauzac Wind Tunnels Department, ONERA, France, Nov. 1998.

[20] Allen, H.J., and Vincenti, W.G., "Wall Interference in a Two-Dimensional-Flow Wind Tunnel, with Consideration of the Effect of Compressibility," NACA Report 782, 1944.

[21] Abbott, I.H., and von Doenhoff, A.E., *Theory of Wing Sections*, Dover Publications, pp. 124-128 and 498-499, 1959.

[22] McCullough, G.B., and Gault, D.E., "Examples of Three Representative Types of Airfoil-Section Stall at Low-Speed," NACA TN-2502, Sept. 1951.

[23] Drela, M., and Youngren, H. "XFOIL 6.96 User Guide," Aeronautical and Astronautical Engineering, Massachusetts Inst. of Technology, Cambridge, MA, 10 March 2001.

[24] Ladson, C.L., "Effects of Independent Variation of Mach and Reynolds Numbers on the Low-Speed Aerodynamic Characteristics of the NACA 0012 Airfoil Section," NASA TM-4071, Oct. 1988.

[25] Kim, H.S., "Effect of Leading-Edge Ice Accretion Geometry on Airfoil Performance," M.S, Thesis, Dept. of Aeronautical and Astronautical Eng., Univ. of Illinois, Urbana, Illinois, 2004.

[26] Lee, S., and Bragg, M.B., "Investigation of Factors Affecting Iced-Airfoil Aerodynamics," *Journal of Aircraft*, Vol. 40, No. 3, May-June 2003, pp. 499-508.

[27] Cabler, S.J.M., "Aircraft Ice Protection," Federal Aviation Administration Advisory Circular, AC No. 20-73A, Aug. 16, 2006.

[28] Broeren, A.P., Bragg, M.B., and Addy, H.E., Jr., "Flowfield Measurements About an Airfoil with Leading-Edge Ice Shapes," *Journal of Aircraft*, Vol. 43, No. 4, July-Aug., 2006, pp. 1226-1234.

[29] Jones, B.M., "An Experimental Study of the Stalling of Wings," Aeronautical Research Committee Reports and Memoranda, No. 1588, Dec. 1933.

[30] Tani, I., "Low-Speed Flows Involving Separation Bubbles," *Progress in Aeronautical Sciences*, Vol. 5, No. 2, 1964, pp. 70-103.

[31] Kerho, M.F., and Bragg, M.B., "Airfoil Boundary-Layer Development and Transition with Large Leading-Edge Roughness," *AIAA Journal*, Vol. 35, No. 1, Jan. 1997, pp. 75-84.